Application of spectropolarimetry to cloud ice measurements in the LWIR

Kira Ann Hart
Comprehensive Exam, Fall 2019
Wyant College of Optical Science, University of Arizona, Tucson, AZ 85721 , USA
khart@optics.arizona.edu

Abstract: Polarimetric measurements of ice clouds in the LWIR are are necessary to constrain ice cloud microproperties to build global cloud dynamic and distribution models. However, the design of long-wave infrared (LWIR) polarimeters pose significant optical engineering challenges. To motivate this technology, the physical phenomena which produce partially linear polarized light in the LWIR are described. An infrared channeled spectropolarimeter (IRCSP) approach is chosen to produce snapshot full linear Stokes measurements within a small form factor.

1 Introduction

Until recently CubeSat sized long-wave infrared (LWIR) polarimeters were not feasible due to detector cooling requirements. While uncooled microbolometer detectors have opened the door for LWIR polarimetric imaging, the optical design of compact instruments capable of producing precise linear Stokes measurements poses considerable optical design and data reduction challenges. To meet the requirements for spaceflight, an InfraRed Channeled Spectro-Polarimeter (IRCSP) is evaluated. [1] A channeled polarimeter modulates polarization as a function of wavelength without any moving components encoding polarization information as spectral intensity. Once deployed, the IRCSP will produce the first linear Stokes measurements of cirrus ice clouds in the LWIR . [2] Due to the large potential wealth of data available from polarimetry, both passive and active polarimetric measurements of cirrus clouds in reflection and transmission have been performed in the near IR and microwave bandwidths. However, shorter wavelength polarimetric measurements are necessary to probe crystals of smaller diameters in order to decode the full microphysical information. [3, 4] This manuscript describes the application of a channeled spectro-polarimetric method to produce the needed linear Stokes measurements within a form factor suitable for CubeSat deployment.

2 Polarized Light Phenomenology

2.1 Polarized Light and Stokes Parameters

The polarization of a light field describes the direction of oscillation of the transverse electric field. While all monochromatic light is fully polarized, broadband light can be fully, partially, or un - polarized. The Stokes parameters uniquely quantify the polarization state of incoherent light with four real numbers, $[S_0, S_1, S_2, S_3]$. While the real valued Stokes parameters do not contain information about absolute phase of the light, they do describe the degree

of polarization. The normalized Stokes vectors are described

$$\begin{bmatrix} I/I \\ Q/I \\ U/I \\ V/I \end{bmatrix} = \begin{bmatrix} s_0 \\ s_1 \\ s_2 \\ s_3 \end{bmatrix} = \frac{1}{P_H + P_V} \begin{bmatrix} 1 \\ P_H - P_V \\ P_{45^\circ} - P_{135^\circ} \\ P_R - P_L \end{bmatrix} \tag{1}$$

where the P_i terms represent radiance measurements through ideal polarizers. The linear polarization measurements H, V, 45° and 135° depend of the choice of coordinate system. The circular measurement R and L do not depend on the choice of coordinate system since they represent the handedness of the light relative to its propagation direction. Any two orthogonal states, H-V, 45°- 135°, or R-L can be combined in equal parts to form unpolarized light. Together, the Stokes parameters span the full space of possible polarization states called the Poincare sphere [5].

When unpolarized light interacts with a material which has a different response to different polarizations, it becomes partially polarized. Thus by measuring the polarization of light after it interacts with an unknown object, information can be inferred about the object's material and geometric properties. Anisotropy can be introduced by the geometry of a material or by polarization selectivity in atomic absorption and emission. In atmospheric scattering light becomes partially polarized as it interacts with optical interfaces of varied geometries. As there are no significant mechanism by which light becomes circularly polarized in atmospheric scattering, the s_3 term is negligible. As a result only two parameters are needed to describe the the polarization of atmospheric scattering. The angle of linear polarization (AoLP) describes the angle of the polarization vector with respect to a local coordinate system, and degree of linear polarization (DoLP) describes what fraction of the light field is polarized. [5]

$$\text{AoLP} = \frac{1}{2}\tan^{-1}\left(\frac{s_2}{s_1}\right) \quad , \quad \text{DoLP} = \frac{\sqrt{s_1^2 + s_2^2}}{s_0}. \tag{2}$$

2.2 Light Matter Interaction in the LWIR

The complex refractive index $\tilde{n} = n + i\kappa$ describes both the phase velocity $n = c/v$ and the attenuation constant κ for a material. Both liquid and ice water are dielectrics; light propagates through the media as the field couples to electric dipoles. In regimes far off from any molecular or electronic resonances, this light matter interaction is described by the Lorentz Oscillator model; the light field drives electrical polarization within the material analogous to classical mechanical springs. These dipoles in turn re-radiate photons coherently as the field propagates though the medium. The refractive index depends on wavelength, as the system will have a larger amplitude of oscillation when the field is close to a resonant eigenfrequency. Regions of anomalous dispersion describe wavelengths where the frequency of light is on resonance to drive electronic transitions or vibrational excitation and κ spikes. In regions near electronic

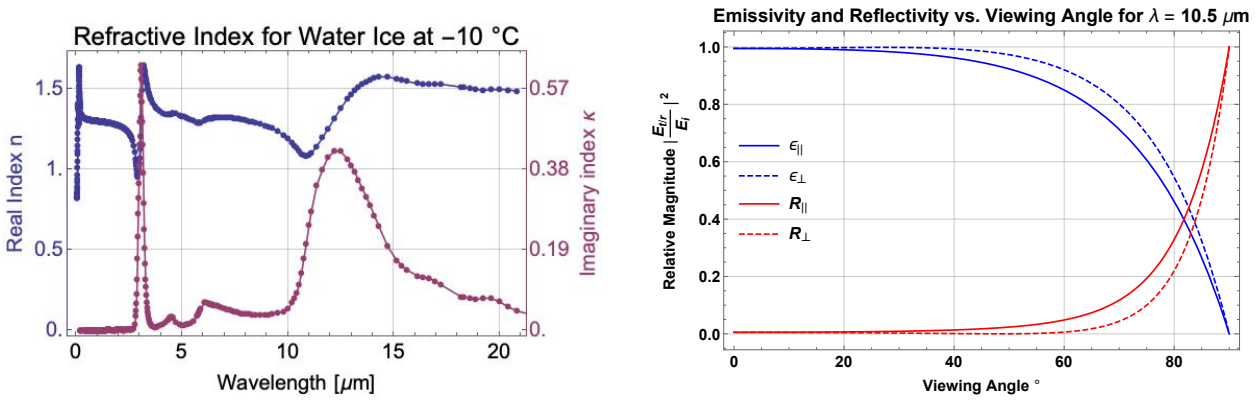

(a) (b)

Figure 1: (a) shows the imaginary and complex components of the refractive index of ice as a function of wavelength. (b) shows the Fresnel coefficients for 10 μm calculated using Equation 5 as a function of angle of incidence

resonances, the field is more likely to be excite an electron into a higher energy level, absorbing energy from the light field. In regions of normal dispersion, the refractive index is predominantly real. Figure 1a shows that for ice, anomalous dispersion occurs for a resonances at 3 μm and between 10 - 15 μm where there are peaks in the imaginary component of the refractive index. In the infrared, light drives vibrations on the molecular scale. This causes LWIR light to be absorbed through the optical excitation of phonons, quasi particles which describe thermal "vibration waves" in a material. Phonons are created when energy is removed from the light field and converted into vibrational energy between adjacent lattice points in a crystal. These thermal vibrations form a collective periodic excitation in the medium. When the wavelength of light is long in comparison to the size of the crystal lattice, energy of the light field is converted into phonons and the temperature of the material increases. This absorption through phonon generation can be seen in the broad peak in the imaginary refractive index between 10 and 15 μm in Figure 1a. This phenomena is why the LWIR is often called the thermal IR. Electromagnetic waves at this wavelength transfer thermal energy from one material to another through free space though the generation of phonons.

Ice particles have a hexagonal crystal structure which produces an mildly anisotropic refractive index; light at the same wavelength will observe a different refractive index depending on its polarization. However, the anisotropy of ice formed at temperatures in the Earth's atmosphere is negligible. The dominant source of polarizance in ice crystal interaction arises from Fresnel interactions at optical interfaces. As the angle of incidence θ relative to the surface normal increases, the projection of the fields in the transverse plane onto the interface will have different magnitudes parallel and perpendicular to the surface normal. The Fresnel coefficients represent the relative magnitude of the field in reflection and transmission compared to the incident field $|E_{r,t}/E_i|^2$. The coefficients for light polarized parallel and perpendicular to the plane of incidence are

$$R_{\parallel} = \left|\frac{n_i \cos\theta_t - n_t \cos\theta_i}{n_i \cos\theta_t + n_t \cos\theta_i}\right|^2, R_{\perp} = \left|\frac{n_i \cos\theta_t - n_t \cos\theta_t}{n_t \cos\theta_i + n_i \cos\theta_t}\right|^2, T_{\parallel} = \left|\frac{2n_i \cos\theta_i}{n_i \cos\theta_t + n_t \cos\theta_i}\right|^2, T_{\perp} = \left|\frac{2n_i \cos\theta_i}{n_t \cos\theta_i + n_i \cos\theta_t}\right|^2 \quad (3)$$

where n_i and n_t are the incident and transmitted refractive indices respectively, θ_i is the angle of incidence, and $\theta_t = \arcsin(n1/n2 \sin\theta_i)$ is the transmitted angle given by Snell's Law . Figure 1b shows the squared Fresnel intensity coefficients for 10.5 μm light as a function of the viewing angle.

2.3 Kirchoff's Laws for Polarized Radiation

A blackbody is an idealized cavity which absorbs all radiation incident upon it. In thermal equilibrium, a blackbody at temperature T will emit light with spectral radiance is described by Planck's Law

$$u(\nu, T) = \frac{8\pi\nu^2}{c^3} \frac{h\nu}{e^{h\nu/kT} - 1} \tag{4}$$

where ν is the frequency of the emitted radiation, k is the Boltzmann constant, and h is Planck's constant. This radiation is produced by quantized modes separated by $E = h\nu$ within the cavity. While more modes are available at higher frequencies, the quantized nature of electromagnetic radiation dictates that they require more energy to excite and are thus less probable. The radiation profile of most thermal sources is well described by Planck's law. At room temperature radiance peaks at $\lambda_{peak} \approx 10\ \mu m$. In practice, all targets in a terrestrial scene produce peak radiation in the LWIR. Emission from a perfect blackbody is unpolarized. Since an ideal blackbody absorbs all incoming radiation, to satisfy the conservation of energy it must emit radiation without preference. In the physical world α is always less than 1 and the emitted light will exit the media partially polarized. For these "greybody" radiators, the Fresnel coefficients describe the amount of internally emitted radiation that is transmitted as opposed to reflected back into the media.

Consider looking down upon a piece of ice with a thickness much greater than its optical depth such that all light incident from below it has been attenuated ; it appears opaque. In this case, all light observed will have either been reflected from the upper surface, or emitted from the ice itself. Figure 2 shows the DoLP and AoLP of light emitted and reflected from ice as a function of viewing angle. The AoLP and DoLP of light measured is dependent upon the relative radiance of the fields reflected and emitted by the object. If the emitting object T_o is much hotter than the background environment T_b, the polarization signature will be dominated by and emission polarization. When the $T_b << T_o$, the polarization is dominated by reflection. In LWIR polarimetry the same object will have a different polarization signature depending on its temperature relative to the background scene.

2.4 Particle Geometry

The polarization of light exiting an ice crystal is also dependent upon its geometry. The ice particles in cirrus clouds have diameters D of between 20 and 200 μm. The scattering parameter $a = \pi D/\lambda$ informs which scattering regime describes the interaction. In the LWIR, ice crystals have a scattering parameter $7.8 < a < 78$. Mie scattering is applied to problems with $a \approx 1$, so for the smallest particles a full-wave simulation approach should be employed to capture

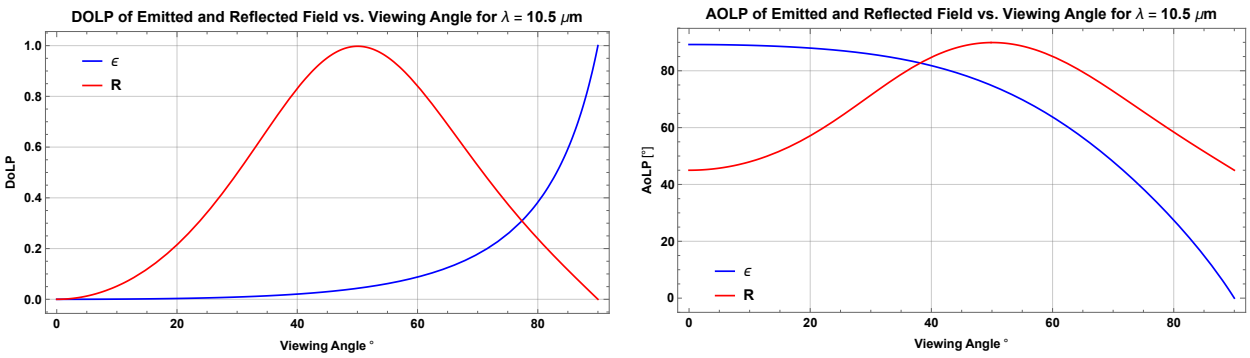

(a) (b)

Figure 2: (a) shows the DoLP and (b) shows the AoLP of light reflected and emitted from a flat ice surface as a function of viewing angle

diffraction effects. However, since all particles have $a > 1$ in the LWIR, a geometric ray tracing approach is appropriate to gain a phenomenological understanding of how crystal geometry contributes to the polarization signal. Figure 3a shows collimated light entering a spherical ice crystal. Light that enters the crystal off axis enters the sphere with a higher angle of incidence as seen in Figure 3. Thus, off axis light will show polarization preferential transmission. This phenomena is called diattenuation and is described

$$D = \frac{T_{max} - T_{min}}{T_{max} + T_{min}}. \tag{5}$$

The values T_{max} and T_{min} correspond to the states with maximal and minimal transmission, respectively. Figure 3c shows that light entering the sphere at its edges will be more polarized than the light transmitted on axis through the center of the crystal. As the field continues to interact with more crystal interfaces, these effects will compound. The resulting angle and degree of linear polarization will change depending on the shape, size, and dynamics of the ice particles in the path of the light. Though out of the scope of this paper, geometric ray tracing models using the optical properties of ice discussed here can be applied to radiative transfer models to discriminate between different polarization states exiting ice clouds in the LWIR.

3 Channeled Polarimeter Design

A channeled spectro-polarimeter is utilized to measure the spectrally dependent AoLP and DoLP in a compact instrument. To measure polarization, the light field polarization must be modulated by some mechanism to be measured as intensity. For example, rotating a linear polarizer in front of a beam will measure the amount of power projected in each linear polarization state. For compact space based applications, it is ideal to eliminate the need for rotating components and image the full space of linear stokes parameters in a single snapshot. A channeled spectro-polarimeter

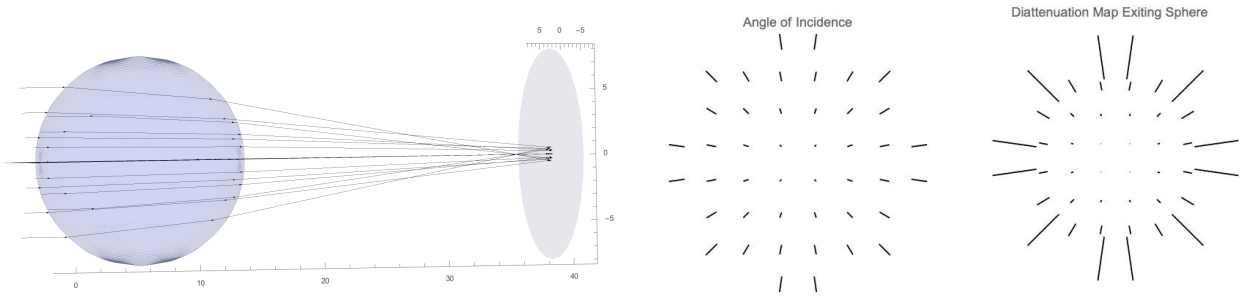

(a) (b) (c)

Figure 3: (a) shows a collimated grid of 10.5 μm rays entering a spherical ice crystal. (b) shows an AOI map of rays entering the first surface with a maximum scale corresponding to $\theta = 68°$ (c) shows the a diattenuation map of the rays exiting the sphere with a maximum scale of 0.06.

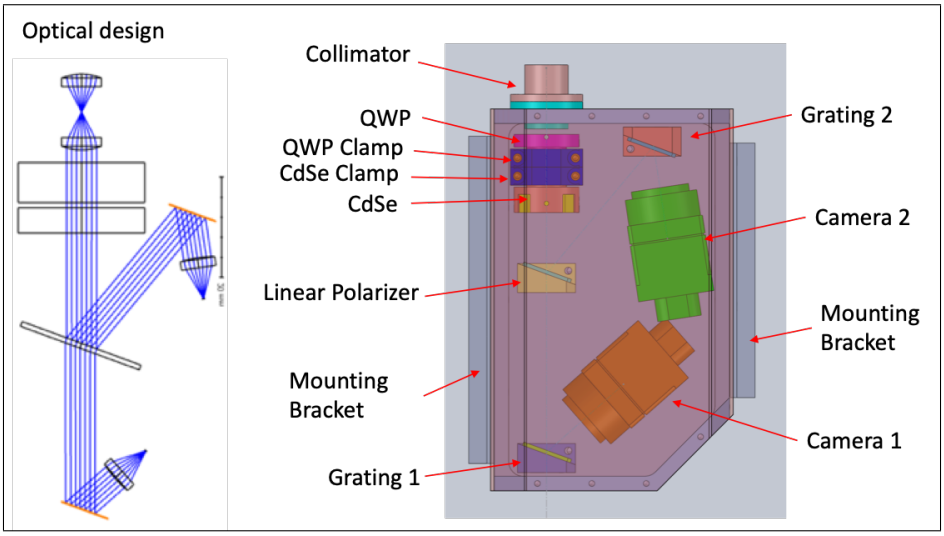

Figure 4: Optical design of the IRCSP

accomplishes this by modulating the polarization state as a function of wavelength instead of in time. The IRCSP is comprised of collimating lenses, birefringent optical elements, and a linear polarizer followed by a diffraction grating and imaging lens, to image a polarization spectrum at the focal plane. To introduce a wavelength dependent frequency to the spectral signal , the incoming linear polarization is first rotated as a function of wavelength. This operation is performed by a quarter wave retarder (QWR) with a fast axis at 45° followed by a CdSe crystal high order retarder (HOR) which together act as wavelength-dependent circular retarder. In the SWIRP instrument the rotated polarized light is then modulated by a wiregrid linear polarizer (LP) tilted at 20°, which separates the 45° and 135° polarization states into two different paths. The measurement of both the reflected and transmitted paths by the LP enables the distinction between wavelength dependent transmission the degree of polarization. Added together the two orthogonal spectra measure the spectral radiance of the target. [1]

Unpolarized light has its polarization state unchanged by the QWR and HOR, so one half of the flux exits the LP in

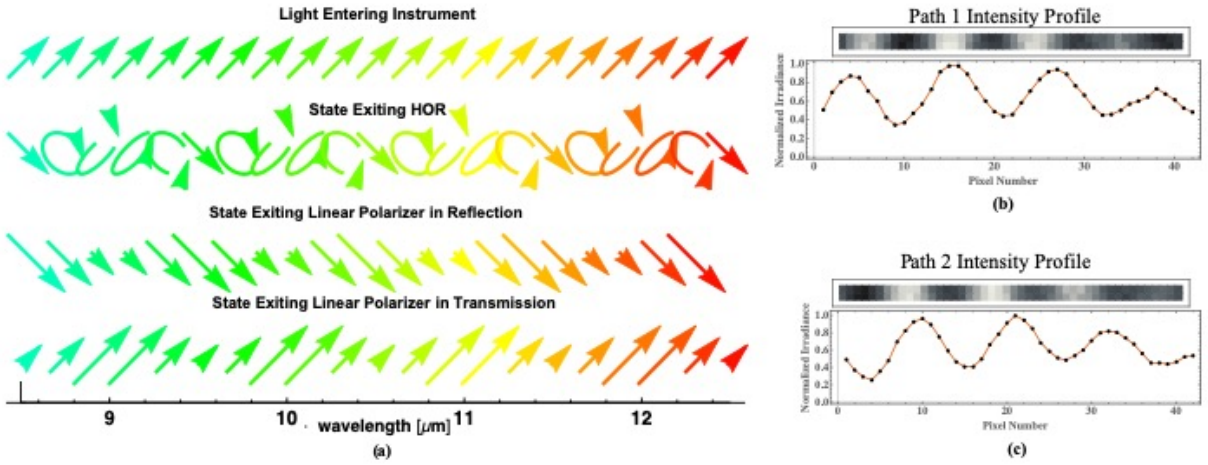

Figure 5: Visualization of the operation of the IRCSP Mueller matrix model on linearly polarized light of varying DoLP and AoLP. (a) shows the how the polarization is altered as a function of wavelength as it passes through the quarter wave-plate and high order retarding CdSe crystal. Following the HOR the beam is split and modulated by a linear polarizer . Following the linear polarizer are 2 separate diffraction gratings and detectors which serve as the spectrometer. (b) and (c) shows the produced modulation patterns imaged onto the detector.

each outgoing polarization beam for all wavelengths. When linearly polarized light is incident, the output polarization from the QWR and HOR is rotated as a function of the wavelength, as shown in Figure 5. Then, the LP modulates the transmitted and reflected intensity as a function of wavelength with a modulation period of 1 μm with opposite polarities in path 1 and path 2. The modulation period corresponds to a spectral retardance variation of one wave per μm, which prescribes the length of the HOR, since the specified resolution of the polarization measurement is a 1-μm bandpass centered at 11 μm. The amount of modulation is proportional to the DoLP, and the phase of the modulation describes the AoLP. Thus in this design, the DoLP and AoLP are measured with 1-μm resolution, as rapid variation with wavelength is not expected. Finally, the diffraction grating and imaging lens image a 46x2 array spectral for each polarization channel, 46 for the spectral sampling and 2 for spatial sampling. For each snapshot, the polarimeter produces a spectral and radiometric polarization measurement for a 2 pixel area. Once deployed, the instrument will be operated in a push-broom pattern to form mosaic polarization images in 2 pixel steps.

4 Uncooled Microbolometers

In order to measure the light collected by the optics, the light field must be converted into an electrical signal. Due to their speed, photon detectors are popular in the visible. Photon detectors generate an electrical signal when an incident photon frees a bound electron, creating an electron-hole pairs in a semiconductor. These carriers produce a measurable electrical current when a bias voltage or current is applied. In the thermal IR at room temperature, the detecting material and housing itself is emitting photons at the same wavelength it is trying to detect, washing out the

(a) (b)

Figure 6: (a) shows a single uncooled microbolometer pixel. A large current and low voltage is applied across the absorbing material (VOx) and connected to substrate ROIC [6]. (b) shows the compact form factor of FLIR's uncooled microbolometer named the "Boson" [6].

signal incident on the focal plane. Thus, to use photon detectors in the LWIR, the detectors must be cooled to a point where they will not emit a significant amount of IR radiation, requiring large and costly dewer cooling systems. So while photon detectors are ideal for highly sensitive and fast detection, their intense space and power requirements are limiting for rapid deployment or compact spaceflight applications. To achieve LWIR imaging at room temperature, a different light-matter interaction must be measured.

The optical excitation of phonons through the absorption of infrared radiation discussed in section 2.2 produces an material effect which can be used to measure the light field. Electrical resistance R is delay caused by the scattering of electrons as they attempt to move through a material. When phonons are present ($T > 0K$), electrons encounter additional sources of scattering, increasing the resistance of the material. As more phonons are created the probability of an electron encountering a phonon increases and the resistance thus increases. Bolometers are detectors which use change in resistance across an absorbing material to measure in intensity of the IR light incident upon them. While the first bolometer was invented in the late 1800's, producing bolometer detectors with pixels small enough to achieve imaging resolution with high sensitivity at room temperature was not possible until recently. Uncooled microbolometers (UMBs) incorporate an infrared absorbing material into a Read Out Integrated Circuit (ROIC) as seen in Figure 6a. A reflective layer below the absorbing material enhances sensitivity by double passing incident radiation through the absorbing material, and the legs provide the thermal isolation necessary to place many pixels close to one another and reduce crosstalk. The UMB used in the IRCSP is FLIR's Boson (Figure 6b), which has a pixel pitch of only 12 μm.

The main source of noise in an UMBs is caused by Johnson noise E_j, which describes the random motion of carriers in a circuit. It takes the functional form

$$E_j = (4kTR\Delta f)^{1/2}V \tag{6}$$

where k is Boltzmann's constant, T is the temperature, R is the resistance, Δf is the bandwidth of the circuit, and V is the voltage . Because bolometers measure a change in resistance, it is possible to construct a circuit with constant voltage and measure change in current or vice versa. However, to minimize Johnson noise it is ideal to utilize a constant low voltage and measure the change in current across the pixel , $I(R) = V_c/R$. To produce a measurable signal, the radiation incident on the focal plane must generate a change in resistance which produces a change in current greater than that of the intrinsic noise. This minimum resolvable difference is called the Noise Equivalent Differential Temperature , or NEDT. Remarkably, the compact Boson achieves an NEDT $< 50mK$, enabling precise measurements at room temperature.

5 Data Reduction

The modulated signal at the focal plane for paths 1 and 2 will have the functional form

$$I_{1/2}(\lambda) = \frac{A(\lambda)}{2}\left(1 \pm D\sin(\varepsilon\lambda - 2\theta)\right) \tag{7}$$

where A is the spectral irradiance at the detector, ε is carrier frequency produces by the retardance variation introduced by the HOR, D is the DoLP and θ is the AoLP. Figure 7a shows the resulting signal generated by paths 1 and 2 with fixed pattern expected from Johnson noise added. The data reduction to determine A, D and θ is performed in Fourier space

$$\mathscr{F}\{I_{1/2}(\lambda)\}(\xi) = \frac{A}{2}\left[\delta(\xi) \pm De^{2\theta i}\left[\delta(\xi-\varepsilon) + \delta(\xi+\varepsilon)\right]\right]. \tag{8}$$

The amplitude of both the real and imaginary components of $\mathscr{F}\{I_{1/2}(\lambda)\}(\xi)$ at $\xi = 0, \pm\varepsilon$ in each path form a system of equations which are solved for A, D, and θ where A is described by the magnitude of the DC term, D describes the magnitude of the carrier frequency ε term, and the exponential changes the relative magnitude of the real and imaginary parts of the Fourier transform as a function of θ. In practice, we have a discrete signal I_n and thus take a discrete Fourier transform (DFT)

$$c_k = \sum_{n=0}^{N-1} I_n \cdot e^{i\frac{2\pi kn}{N}} \tag{9}$$

where N in the length of the signal. To achieve 1 μm resolution, the signal is truncated in 1 μm windows. Since the carrier frequency introduced by the CdSe is $1\mu m^{-1}$, the c_0 term in the DFT contains the DC term $\frac{A}{2}$, and the c_1 term contains the carrier frequency term $\frac{A}{2}De^{2\theta i}$ as seen in Figure 7. Because the fixed pattern noise expected from the detector has a high spatial frequency compared to the period of modulation, noisy contributions will appear in larger frequency terms of the DFT. Thus, performing the data reduction in Fourier space helps reduce the effects of noise in the system.

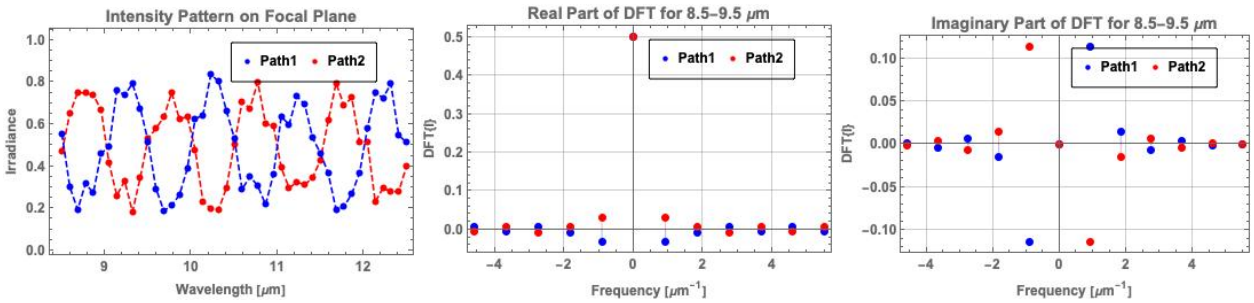

(a) (b) (c)

Figure 7: (a) shows the signal generated by each path for $D = 0.5$, $\theta = 0$, and $A = 1$ (b)hows the real part of the DFT from (a) for the signal truncated between 8.5 - 9.5 μm. (c) shows the imaginary component of the DFT

6 Conclusion

The advent of high resolution, low NEDT uncooled microbolometers has enabled the optical design of a LWIR polarimeter with a CubeSat suitable form factor and power requirement. Because a channeled polarimeter does not require any moving components, the IRCSP design further reduces the risk involved in launching and maintaining space based optical instruments. Deployed, this instrument will produce the first full linear Stokes measurements of cirrus ice clouds in the LWIR. These measurements will provide information about the microphysical properties of cloud ice particles which are crucial to constrain current climate models. While designed for cloud-ice measurement, the IRCSP's form factor and cost make it a candidate for a variety of future thermal polarimetric sensing applications including ocean surface normal estimation, atmospheric monitoring of aerosols, and spectro-polarimetric fingerprinting for target identification.

References

[1] K. A. Hart, R. A. Chipman, and D. L. Wu, "Compact lwir polarimeter for cirrus ice properties," **10655**, 2018.

[2] ESTO, *ESTO 2016 Report*, NASA, 2016.

[3] J. Gong and D. L. Wu, "Microphysical properties of frozen particles inferred from global precipitation measurement (gpm) microwave imager (gmi) polarimetric measurements," *Atmospheric Chemistry and Physics* **17**(4), pp. 2741–2757, 2017.

[4] J. Miao, K.-P. Johnsen, S. Buehler, and A. Kokhanovsky, "The potential of polarization measurements from space at mm and sub-mm wavelengths for determining cirrus cloud parameters," *Atmospheric Chemistry and Physics* **3**(1), pp. 39–48, 2003.

[5] R. A. Chipman, T. Lam, and G. Young, *Polarized Light and Optical Systems*, CRC Press, New York, 2019 (first edition).

[6] J. Hecht, "Photonic frontiers: Room-temperature ir imaging: Microbolometer arrays enable uncooled infrared camera," *Laser Focus World* , 2012.